ACS OMEGA

http://pubs.acs.org/journal/acsodf

Article

Unveiling the Performance of Cu−Water Nanofluid Flow with Melting Heat Transfer, MHD, and Thermal Radiation over a Stretching/Shrinking Sheet

Arfan Hyder, Yeou Jiann Lim,* Ilyas Khan, and Sharidan Shafie

Cite This: *ACS Omega* 2023, 8, 29424−29436

Read Online

ACCESS | Metrics & More | Article Recommendations

ABSTRACT: The use of melting heat transfer (MHT) and nanofluids for electronics cooling and energy storage efficiency has gained the attention of numerous researchers. This study investigates the effects of MHD, mixed convection, thermal radiation, stretching, and shrinking on the heat transfer characteristics of a Cu−water-based nanofluid over a stretching/shrinking sheet with MHT effects. The governing equations are transformed into nonlinear ordinary differential equations and solved numerically using the Keller Box method. To the best of our knowledge, this comprehensive analysis, encompassing all of these factors, including the utilization of a robust numerical method, in a single study, has not been previously reported in the literature. Our findings demonstrate that an increase in the melting parameter leads to an enhanced rate of heat transfer, while an increase in the stretching/shrinking parameter results in a decrease in the rate of heat transfer. Additionally, we present a comprehensive analysis of the influences of all of the mentioned driving parameters. The results are presented through graphical and tabulated representations and compared with existing literature.

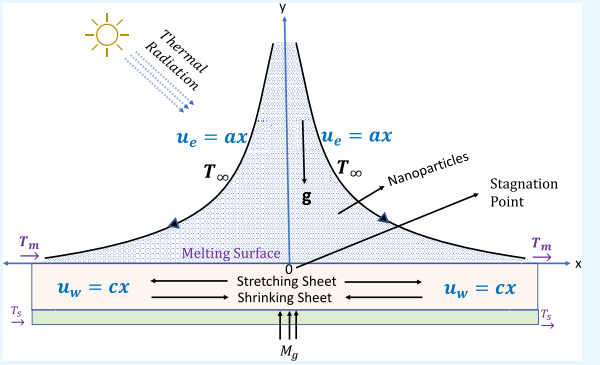

1. INTRODUCTION

Nanofluids represent a state-of-the-art category of fluids that are utilized for the solutions of nanomaterials with exceptional thermal conductivity properties. These fluids are ideal for heat transfer applications. The emergence of nanotechnology has enabled the creation of these fluids, which are composed of nanoparticles that are typically 50−100 times smaller than the diameter of a human hair. This remarkable reduction in particle size contributes to their unique thermal properties and makes them a promising innovation in the field of heat transfer fluids. As a result of their small size, nanomaterials exhibit distinct properties that make them ideal for various applications. In 1995, Choi and Eastman[1] originated the idea of using nanocomposites to improve heat transfer in liquids, which led to the concept of nanofluids. Researchers have since been exploring different methods for synthesizing and characterizing nanofluids, including the use of various nanoparticles and base fluids.

Recent research suggests that nanofluids exhibit potential as a replacement for conventional single-phase fluids in a wide range of heating and cooling applications. Their adaptability enables their use in various fields such as solar collectors, biomedical devices, and electronics cooling which has sparked significant interest in both academic research and industrial applications.[2] Despite the challenges involved in developing nanofluids, their potential to revolutionize various industries such as desalination processes, enhancing porous media, improving aerospace technology, capturing CO_2 emissions, optimizing liquid-based heat exchangers, and increasing efficiency in oil recovery makes them a promising area of research.[3] The article by Chakraborty and Panigrahi[4] offers an extensive assessment of nanofluid stability, encompassing all stages from preparation to application. The focus of the review is to examine the stability of nanofluid in various operating conditions, which may include high temperature, pressure, confinement, composition, exposure to saline environments, and the presence of external magnetic fields. The recent study by Li et al.[5] regarding the thermal conductivity of nanofluids was reviewed, with a focus on the emergence of new types of nanofluids that exhibit enhanced thermal conductivity. The paper also discusses efficient prediction models for thermal conductivity and covers the influencing factors, prediction models, and applications of nanofluids. Extensive research has been conducted on nanofluids for their use in manufacturing and engineering fields, particularly as heat transfer fluids.[6]

Received: April 29, 2023
Accepted: July 4, 2023
Published: July 31, 2023

These fluids, which contain nanoparticles, offer numerous benefits in various applied fields. Researchers have investigated various aspects of nanofluids, including improving thermal conductivity, incorporating nanoparticles, and other related areas.[7]

Melting heat transfer (MHT) is an important mechanism in various industrial processes, including manufacturing of semiconductors, metal casting, soil thawing and freezing, and energy storage. The concept of MHT was initially proposed by Roberts[8] in 1958 to describe the melting process of a solid material in contact with a hot fluid, and since then, significant contributions have been made to the field by researchers. The early work of Yen and Tien[9] on laminar heat transfer over a melting surface is a notable contribution to the research of melting heat transfer. Recent research has been focused on increasing the efficiency of energy storage through latent heat and exploring the possibilities of MHT in electronics cooling, welding, etc. MHT is a critical process in numerous manufacturing processes, including permafrost melting, electromagnetic induction furnaces, polymer synthesis, laser ablation, coil exchangers, and more. The ongoing research has the potential to lead to further improvements in technology. Therefore, the current study holds great importance not only in industrial applications but also in the development of chemical and biomedical products.[10] However, simulating MHT is challenging due to the coupling between fluid dynamics and the moving interface, which is referred to as a "Stefan moving boundary" problem. The development of advanced computational techniques has been crucial in accurately and efficiently solving these complex problems.[11,12]

Stretching and shrinking of sheet flow has been extensively studied due to its relevance in various industrial processes such as paper production, glass manufacturing, metal containers, polymer processing, and quality control among others.[13] Research has been carried out to investigate the characteristics of fluids in the vicinity of a surface that is either being stretched or contracted in depth by numerous researchers, following the pioneering work of Sakiadis[14] in 1961. He conducted the initial research on the equations that govern the boundary layer of continuous solid surface flow, in both their two-dimensional and axisymmetric forms. Extensive studies have been conducted on the behavior of continuously stretched or moving surfaces under various fluid conditions, with a focus on heat transfer and considering a wide range of boundary conditions and physical factors.[15] The fluid flow and heat transfer characteristics of thermally processed sheet-like materials are sensitive to stretching or shrinking, which can significantly impact the quality and efficiency of the production process. As a result, extensive research has been conducted on sheet flow stretching and shrinking, contributing to the development of efficient and sustainable industrial processes.[16] These investigations have proven invaluable in advancing the understanding of these processes and improving production outcomes, as highlighted in a study on melting by Uddin et al.[17] The study conducted by Mondal and Bharti[18] investigated the impact of MHD on the transfer of heat and mass in a nanofluid, taking into account heat generation or absorption, under a stagnation boundary layer flow over a stretching or shrinking sheet. Jumana et al.[19] explored the impacts of mixed convection and MHD effects on the performance of a nanofluid across a stretched or contracting sheet. Furthermore, the melting heat transfer near the surface showed that the thickness of the thermal boundary layer and the nondimensional temperature near the surface were reduced significantly by the melting parameter. The investigation conducted by Pop et al.[20] analyzed the stagnation point and thermal behavior of a nanofluid that passes over a sheet undergoing either stretching or shrinking. The study examined the effects of several influential factors, such as MHD, melting, second-order slip, and suction, on the nanofluid's stagnation point and thermal behavior. The characteristics of heat transfer and stagnation point flow of a nanofluid over a melting stretched sheet in a laminar flow environment containing a warm liquid were studied by Kishore Kumar and Bandari.[21] The research mainly focused on a two-dimensional scenario and aimed to shed light on how melting affects the heat transmission process. Gireesha et al.[22] conducted research utilizing numerical simulations to explore a 2-dimensional flow at a stagnation point over a stretching surface, in an electrically conducting nanofluid. The study comprehensively examined the influence of various parameters, including melting, heat production or absorption, and an induced magnetic field.

The critical factors considered in our study are highly significant in the existing literature. For example, we have chosen to work with a water-based nanofluid, incorporating copper nanoparticles to enhance its thermal conductivity to 400 W/m K.[23] This addition of nanoparticles is expected to significantly improve the heat transfer efficiency of the Cu-nanofluid, making it a promising option for various applications.[24] MHD finds relevance in a wide range of disciplines, including physics, astronomy, solar physics, laboratory studies, medical applications, manufacturing, and engineering.[25,26] Additionally, the importance of thermal radiation in contemporary technological and industrial contexts cannot be overlooked. An important practical application is the utilization of solar radiation as an energy source on Earth. Numerous researchers are currently investigating the impact of thermal radiation on different fluids under varying conditions.[27] To ensure accurate results, we have employed a numerical approach Keller Box known for its robustness, unconditional stability, and ability to solve models with high precision.[28] While previous research has primarily focused on analyzing individual factors or their combinations in specific scenarios, our study takes a comprehensive approach. Inspired by previous studies, our aim is to investigate the flow and heat transfer properties of a Cu−water nanofluid at a stagnation point. We consider the combined effects of multiple factors, including MHD, thermal radiation, and mixed convection parameters, within the framework of melting heat transfer over a stretching or shrinking sheet, which distinguishes our study. By analyzing these complex interactions, our research aims to provide valuable insights into their collective influence.

The novelty of this study lies in its focus on nanofluid with melting, stretching, shrinking, MHD, thermal radiation, and mixed convection, solved using the Keller Box method, which, to the best of the author's knowledge, has not been explored previously. The study with the included effects holds significant potential for numerous real-life applications, particularly in the domain of thermal energy storage systems. These systems are instrumental in capturing and storing excess thermal energy from diverse sources such as solar or industrial processes, enabling its subsequent utilization. By comprehending the intricate behaviors of nanofluids, phase change materials, and the impacts of stretching or shrinking sheets, researchers can optimize the energy storage capacity, opera-

https://doi.org/10.1021/acsomega.3c02949
ACS Omega 2023, 8, 29424−29436

tional efficiency, and overall thermal management performance of these systems. This advancement paves the way for more efficient and sustainable utilization of thermal energy resources, making a meaningful contribution to various practical applications.[29]

Furthermore, the inclusion of MHD in the model with a very weak strength of the magnetic field. Consequently, the electron-atom collision frequency is assumed to be very low, leading to the neglect of the effects of Hall and ion slip currents.[30−32] Its aim is to examine how a nanofluid behaves in terms of flow and heat transfer as it passes across a sheet that is either stretching or shrinking. A set of ordinary differential equations is obtained by solving the underlying partial differential equations through the use of similarity transformations technique. The present study utilizes the Keller Box method, implemented in MATLAB, to obtain velocity and temperature profiles. The results are expected to provide valuable insights into the fundamental behavior of nanofluid, including controlling parameters, the Nusselt number, and the skin friction coefficient. Additionally, graphical representations and comparison tables will be used to enhance the presentation of the study's findings.

2. GOVERNING EQUATIONS

In the current problem, a steady flow of a nanofluid is considered to approach a sheet that undergoes constant melting into a liquid with similar properties. The sheet is subjected to linear stretching and moves at a velocity of $u_w(x) = cx$, while the external flow has a velocity of $u_e(x) = ax$. In the case of a stretching sheet, c is positive constant, while for a shrinking sheet, it is negative, and a is a positive constant. The melting surface is at a temperature of T_m, while the free-stream temperature is T_∞, which is greater than T_m. Far from the interface, the solid medium has a constant temperature of T_s, where $T_s < T_m$. The geometry is designed to easily depict the model, extending the idea presented by Pop et al.,[20] which is shown in Figure 1. Due to the assumption of a small magnetic

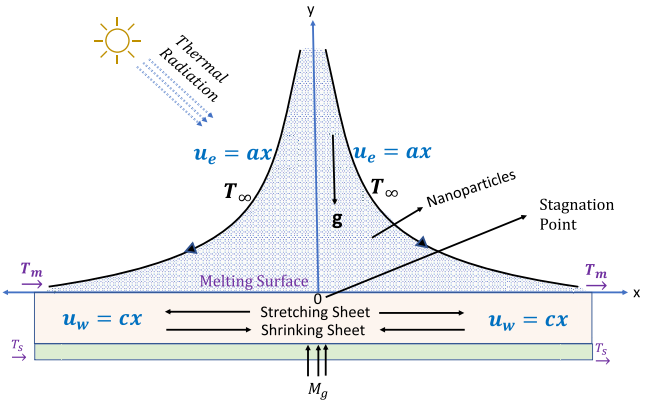

Figure 1. Illustration of the model.

Reynolds number and a weak magnetic field near the stagnation point, magnetic and viscous dissipations are neglected.[33,34] As y is perpendicular to the stretching sheet, the velocity components in the x and y directions are denoted by u and v, respectively. The continuity, momentum, and energy equations are derived, along with magnetic force and radiation heat flux. These equations are then simplified by discarding the irrelevant terms, resulting in the governing equations referred to as[35,36]

Continuity equation:

$$\frac{\partial u}{\partial x} + \frac{\partial v}{\partial y} = 0 \tag{1}$$

Momentum equation:

$$u\frac{\partial u}{\partial x} + v\frac{\partial u}{\partial y} = u_e\frac{\mathrm{d}u_e}{\mathrm{d}x} + \nu_{nf}\frac{\partial^2 u}{\partial y^2} + \frac{(\rho\beta)_{nf}}{(\rho)_{nf}}g(T - T_m) + \frac{\sigma_{nf}}{\rho_{nf}}B_0^2(u_e - u) \tag{2}$$

Energy equation:

$$u\frac{\partial T}{\partial x} + v\frac{\partial T}{\partial y} = \frac{k_{nf}}{\rho_{nf}(C_P)_{nf}}\left(\frac{\partial^2 T}{\partial y^2}\right) - \frac{1}{(\rho C_P)_{nf}}\frac{\partial q_r}{\partial y} \tag{3}$$

The kinematic viscosity of a nanofluid, denoted as ν_{nf}, can be expressed as the ratio of the dynamic viscosity of the nanofluid, denoted as μ_{nf}, to its density, denoted as ρ_{nf}, i.e., $\nu_{nf} = \frac{\mu_{nf}}{\rho_{nf}}$. In addition to these parameters, other factors such as the electrical conductivity denoted as σ_{nf}, the applied magnetic field strength denoted as B_0^2, the thermal expansion of the nanofluid denoted as β_{nf}, and the gravitational acceleration denoted as g also play a role. The temperature of the nanofluid is represented as T, and its thermal diffusivity, denoted as α_{nf}, can be calculated using the thermal conductivity denoted as k_{nf}, and the heat capacity of the nanofluid, denoted as $(\rho C_P)_{nf}$, according to the formula $\alpha_{nf} = \frac{k_{nf}}{(\rho C_P)_{nf}}$. The radiation heat flux, denoted as q_r, expressed in terms of the Stefan−Boltzmann constant, denoted as σ^*, and the Rosseland mean absorption coefficient, denoted as k^*, are written as

$$q_r = -\frac{4}{3}\frac{\sigma^*}{k^*}\frac{\partial T^4}{\partial y} \tag{4}$$

If we expand the T^4 around the constant temperature T_∞ using Taylor Series and neglecting terms of higher order, we obtain the following result

$$T^4 \approx 4T_\infty^3 T - 3T_\infty^4 \tag{5}$$

Using eqs 4 and 5 into eq 3, we get

$$u\frac{\partial T}{\partial x} + v\frac{\partial T}{\partial y} = \frac{k_{nf}}{(\rho C_P)_{nf}}\left(\frac{\partial^2 T}{\partial y^2}\right) + \frac{1}{(\rho C_P)_{nf}}\frac{16}{3}\frac{\sigma^*}{k^*}T_\infty^3\left(\frac{\partial^2 T}{\partial y^2}\right) \tag{6}$$

Following are the initial and boundary conditions for eqs 1, 2, and 6.[35]

$$y = 0: \quad u = u_w(x), \quad T = T_m$$

$$k_{nf}\left(\frac{\partial T}{\partial y}\right)_{y=0} = \rho_{nf}[\lambda + C_s(T_m - T_s)]v(x, 0)$$

$$y \to \infty: \quad u = u_e(x), \quad T = T_\infty \tag{7}$$

https://doi.org/10.1021/acsomega.3c02949
ACS Omega 2023, 8, 29424−29436

3. SIMILARITY TRANSFORMATION

The following similarity transformations are selected to convert eqs 1, 2, and 6 into a set of ordinary differential equations (ODEs).

$$\psi(x, y) = (a\nu_f)^{1/2} x f(\eta), \quad \theta(\eta) = \frac{T - T_m}{T_\infty - T_m}, \quad \eta = y\left(\frac{a}{\nu_f}\right)^{1/2} \tag{8}$$

The stream function $\psi = \psi(x, y)$, which is conventionally expressed as $u = \frac{\partial \psi}{\partial y}$ and $v = -\frac{\partial \psi}{\partial x}$, automatically fulfils the continuity eq 1. After applying these transformations into eqs 2 and 6, we obtained

$$A_1 f''' + A_2(ff'' - f'^2 + 1) + A_3 Ri\theta + A_4 M_g(1 - f') = 0 \tag{9}$$

$$A_5(1 + N_r)\theta'' + A_6 Prf\theta' = 0 \tag{10}$$

The boundary conditions eq 7 becomes nondimensional as

$$\left.\begin{aligned} &f'(0) = \epsilon, \quad \theta(0) = 0, \\ &A_2 Prf(0) + A_5 M_e \theta'(0) = 0, \quad \text{at} \quad \eta = 0. \\ &f'(\eta) = 1, \quad \theta(\eta) = 1, \quad \text{at} \quad \eta \to \infty. \end{aligned}\right\} \tag{11}$$

The notation prime is used to represent differentiation with respect to η. Furthermore, the parameters utilized in this context are defined as follows

$M_g = \frac{\sigma_f B_0^2}{a\rho_f}$ magnetic interaction parameter

$N_r = \frac{16}{3}\frac{\sigma^*}{k^*}\frac{T_\infty^3}{k_{hnf}}$ radiation parameter

$Pr = \frac{\nu_f}{\alpha_f} = \frac{(\mu C_p)_f}{k_f}$ Prandtl number

$Ri = \frac{Gr_x}{(Re_x)^2}$

Richardson number used as the mixed convection parameter

$Gr_x = \frac{g\beta_f(T_\infty - T_m)x^3}{\nu_f^2}$ local Grashof number

$Re_x = \frac{u_e x}{\nu_f}$ local Reynolds number

$M_e = \frac{Cp_f(T_\infty - T_m)}{\lambda + C_s(T_m - T_s)}$ melting parameter

$\epsilon = c/a$ stretching(ϵ>0)or shrinking(ϵ<0)parameter

The melting parameter, denoted as M_e, is determined by a composite of the Stefan numbers for the fluid and solid phases, represented by $C_f(T_\infty - T_m)/\lambda$ and $C_s(T_m - T_s)/\lambda$, respectively. Here, Cp_f denotes the base fluid's heat capacity at a steady pressure.[35]

The constants we derived are as follows

$$A_1 = \frac{1}{(1-\phi)^{2.5}}, \quad A_2 = 1 - \phi + \phi\frac{\rho_s}{\rho_f}, \quad A_3 = 1 - \phi + \phi\frac{(\rho\beta)_s}{(\rho\beta)_f},$$

$$A_4 = 1 + \frac{3((\sigma_S/\sigma_f) - 1)\phi}{((\sigma_s/\sigma_f) + 2) - ((\sigma_s/\sigma_f) - 1)\phi}, \quad A_5 = \frac{k_s + 2k_f - 2\phi(k_f - k_s)}{k_s + 2k_f + \phi(k_f - k_s)}, \quad A_6 = 1 - \phi + \phi\frac{(\rho C_p)_s}{(\rho C_p)_f} \tag{12}$$

The thermophysical parameters for the nanofluid used in different constant parameters are listed in Table 1. The symbol

Table 1. Physical Properties of Nanofluid[19,37,38]

thermophysical properties	nanofluid
dynamic viscosity	$\mu_{nf} = \frac{\mu_f}{(1-\phi)^{2.5}}$
density	$\rho_{nf} = (1-\phi)\rho_f + \phi\rho_s$
thermal conductivity	$k_{nf} = k_f\frac{k_s + 2k_f + 2\phi(k_s - k_f)}{k_s + 2k_f - \phi(k_s - k_f)}$
heat capacity	$(\rho C_P)_{nf} = (1-\phi)(\rho C_P)_f + \phi(\rho C_P)_s$
electrical conductivity	$\sigma_{nf} = 1 + \frac{3((\sigma_S/\sigma_f) - 1)\phi}{((\sigma_s/\sigma_f) + 2) - ((\sigma_s/\sigma_f) - 1)\phi}\sigma_f$
thermal expansion	$(\rho\beta)_{nf} = (1-\phi)(\rho\beta)_f + \phi(\rho\beta)_s$

ϕ is utilized to denote the volume fraction of nanoparticles, and the subscripts for the base fluid $()_f$, nanofluid $()_{nf}$, and solid nanoparticle for copper $()_s$ are used to indicate the respective properties.

Having a formal mathematical representation of crucial dimensionless parameters such as the skin friction coefficient C_f and Nusselt number Nu are essential for their practical applications in engineering and science. This representation enables accurate calculation, design, and optimization of various engineering systems, making it an integral part of the engineering and scientific fields. These representations are given as follows[41]

$$C_f = \frac{\mu_{nf}}{\rho_f u_e^2}\left(\frac{\partial u}{\partial y}\right)_{y=0}, \quad Nu = \frac{xk_{nf}}{k_f(T_\infty - T_m)}\left(\frac{\partial T}{\partial y}\right)_{y=0} \tag{13}$$

After simplification, the locally specified Nusselt number (Nu_x) and skin friction coefficient (C_{fx}) are given as follows

$$C_{fx} = C_f\sqrt{Re_x} = \frac{\mu_{nf}}{\mu_f}f''(0) = A_1 f''(0), \quad Nu_x = (Re_x)^{-1/2}Nu = -\frac{k_{nf}}{k_f}\theta'(0) = -A_5\theta'(0) \tag{14}$$

4. COMPUTATIONAL PROCEDURE: KELLER BOX METHOD

The Keller Box method is a reliable and versatile numerical technique for solving governing equations with boundary conditions. It is known for its high accuracy, flexibility, and

https://doi.org/10.1021/acsomega.3c02949
ACS Omega 2023, 8, 29424−29436

unconditional stability, making it suitable for solving complex problems. Moreover, it can handle equations of any order.[42] To obtain the solution using the Keller Box method, a four-step procedure is followed. First, the differential eqs 9 and 10 are converted to a first-order system. Second, central differences are employed to represent the difference equations. Third, the algebraic equations that result are linearized utilizing Newton's method and expressed as matrix-vector equations. Finally, the linear system obtained is evaluated using the block tridiagonal elimination approach.

4.1. Finite Difference Method. We introduce new dependent variables, $f(\eta)$, $u(\eta)$, $v(\eta)$, $g(\eta)$, and $s(\eta)$, to transform the governing eqs 9 and 10 and boundary conditions eq 11 into a system of first-order differential equations as:

$$f' = u, \quad f'' = v, \quad \theta = g, \quad \theta' = s \tag{15}$$

After applying the new dependent variables described above to transform the governing eqs 9 and 10 into a first-order system, the resulting equations can be represented as follows

$$u' = v \tag{16}$$

$$g' = s \tag{17}$$

$$f' = u \tag{18}$$

$$A_1 v' + A_2(fv - u^2 + 1) + A_3 Rig + A_4 M_g(1 - u) = 0 \tag{19}$$

$$A_5(1 + N_r)s' + A_6 Prfs = 0 \tag{20}$$

The boundary conditions eq 11 are given by

$$\left.\begin{aligned} &\eta = 0: \ u(0) = \epsilon, \quad g(0) = 0, \\ &A_2 Prf(0) + A_5 M_e s(0) = 0, \\ &\eta \to \infty: \ u(\eta) = 1, \quad g(\eta) = 1, \end{aligned}\right\} \tag{21}$$

To apply the numerical method to the first-order system of eqs 16−20, we need to transform it into a nonlinear algebraic system using centered difference derivatives. This involves discretizing the governing equations on a grid of points in the η-plane, which we restrict to a rectangular region of interest. The resulting set of net points describes the discrete approximation as follows

$$\eta^0 = 0; \quad \eta_j = \eta_{j-1} + h_j; \quad j = 1, 2, ..., J; \quad \eta_J \equiv \eta_\infty \tag{22}$$

Here, h_j represents the spacing in the η-direction ($\Delta\eta$-spacing) and j represents the coordinate position. The derivatives such as $p' = \frac{\partial p}{\partial \eta}$ in the η-direction can be approximated using a difference as $\frac{p_j - p_{j-1}}{h_j}$. Similarly, the coordinate points can be represented at the midpoint as $p_{j-1/2} = \frac{p_j + p_{j-1}}{2}$. By centering the approximations on the midpoint, the system of first-order eqs 16−20 can be discretized on the net points to obtain a set of nonlinear algebraic equations as:

$$\frac{u_j - u_{j-1}}{h_j} = \frac{v_j + v_{j-1}}{2} \tag{23}$$

$$\frac{g_j - g_{j-1}}{h_j} = \frac{s_j + s_{j-1}}{2} \tag{24}$$

$$\frac{f_j - f_{j-1}}{h_j} = \frac{u_j + u_{j-1}}{2} \tag{25}$$

$$A_1\left[\frac{v_j - v_{j-1}}{h_j}\right] + A_2\left[\frac{f_j + f_{j-1}}{2}\right]\left[\frac{v_j + v_{j-1}}{2}\right] - A_2\left[\frac{u_j + u_{j-1}}{2}\right]^2 + A_3 Ri\left[\frac{g_j + g_{j-1}}{2}\right] - A_4 M_g\left[\frac{u_j + u_{j-1}}{2}\right] + A_2 + A_4 M_g = 0 \tag{26}$$

$$A_5(1 + N_r)\left[\frac{s_j - s_{j-1}}{h_j}\right] + A_6 Pr\left[\frac{f_j + f_{j-1}}{2}\right]\left[\frac{s_j + s_{j-1}}{2}\right] = 0 \tag{27}$$

4.2. Newton's Method. The discretized set of eqs 23−27 are linearized using the Newton technique as:

$$()_j^{(i+1)} = ()_j^{(i)} + \delta()_j^{(i)}, \quad \text{where} \quad i = 0, 1, 2, 3, \cdots \tag{28}$$

Here, the superscript (i) denotes the i-th iteration of the Newton method, $\delta\,()_j^{(i)}$ is the correction term, and j denotes the coordinate position. After substituting the values of $\delta f_j^{(i)}$, $\delta u_j^{(i)}$, $\delta v_j^{(i)}$, $\delta s_j^{(i)}$, and $\delta g_j^{(i)}$ into eqs 23−27 and neglecting the superscript i and terms of order 2 or greater, by following the procedure outlined, a linear tridiagonal system can be derived as:

$$\delta u_j - \delta u_{j-1} - \frac{h_j}{2}(\delta v_j + \delta v_{j-1}) = (r_1)_{j-1/2} \tag{29}$$

$$\delta g_j - \delta g_{j-1} - \frac{h_j}{2}(\delta s_j + \delta s_{j-1}) = (r_2)_{j-1/2} \tag{30}$$

$$\delta f_j - \delta f_{j-1} - \frac{h_j}{2}(\delta u_j + \delta u_{j-1}) = (r_3)_{j-1/2} \tag{31}$$

$$(a_1)_j \delta v_j + (a_2)_j \delta v_{j-1} + (a_3)_j \delta f_j + (a_4)_j \delta f_{j-1} + (a_5)_j \delta u_j + (a_6)_j \delta u_{j-1} + (a_7)_j \delta g_j + (a_8)_j \delta g_{j-1} = (r_4)_{j-1/2} \tag{32}$$

$$(b_1)_j \delta s_j + (b_2)_j \delta s_{j-1} + (b_3)_j \delta f_j + (b_4)_j \delta f_{j-1} = (r_e qn{:}\ 15)_{j-1/2} \tag{33}$$

where

https://doi.org/10.1021/acsomega.3c02949
ACS Omega 2023, 8, 29424−29436

$$\left.\begin{aligned}
(a_1)_j &= A_1 + \frac{h_j}{2}A_2 f_{j-1/2},\\
(a_2)_j &= \frac{h_j}{2}A_2 f_{j-1/2} - A_1,\\
(a_3)_j &= (a_4)_j = \frac{h_j}{2}A_2 v_{j-1/2},\\
(a_5)_j &= (a_6)_j = -A_2 h_j u_{j-1/2} - \frac{h_j}{2}A_4 M_g,\\
(a_7)_j &= (a_8)_j = A_3 Ri\frac{h_j}{2}.
\end{aligned}\right\} \tag{34}$$

$$\left.\begin{aligned}
(b_1)_j &= A_5(1+N_r) + \frac{h_j}{2}PrA_6 f_{j-1/2},\\
(b_2)_j &= \frac{h_j}{2}PrA_6 f_{j-1/2} - A_5(1+N_r),\\
(b_3)_j &= (b_4)_j = \frac{h_j}{2}PrA_6 s_{j-1/2}.
\end{aligned}\right\} \tag{35}$$

$$\left.\begin{aligned}
(r_1)_{j-1/2} &= u_{j-1} - u_j + h_j v_{j-1/2},\\
(r_2)_{j-1/2} &= g_{j-1} - g_j + h_j s_{j-1/2},\\
(r_3)_{j-1/2} &= f_{j-1} - f_j + h_j u_{j-1/2},\\
(r_4)_{j-1/2} &= A_1(v_{j-1} - v_j) - h_j A_2 v_{j-1/2} f_{j-1/2}\\
&\quad + A_2 h_j (u_{j-1/2})^2 +\\
&h_j A_4 M_g u_{j-1/2} - h_j A_3 Ri g_{j-1/2} - h_j(A_2 + A_4 M_g),\\
(r_5)_{j-1/2} &= A_5(1+N_r)(s_{j-1} - s_j) - h_j PrA_6 s_{j-1/2} f_{j-1/2}.
\end{aligned}\right\} \tag{36}$$

The boundary conditions in eq 21 can be expressed as follows when utilizing the initial guesses.

$$\begin{aligned}
&\delta u_0 = 0, \quad \delta g_0 = 0, \quad A_2 Pr\delta f_0 + A_5 M_e \delta s_0 = 0,\\
&\delta u_J = 0, \quad \delta g_J = 0
\end{aligned} \tag{37}$$

4.3. Block-Elimination Method. The linearized differential eqs 29−33 are solved using the block tridiagonal elimination method. These equations can be expressed as

$$\begin{pmatrix}
[A_1] & [C_1] & & & \\
[B_e qn{:}\ 12] & [A_2] & [C_2] & & \\
 & \ddots & \ddots & \ddots & \\
 & & [B_{J-1}] & [A_{J-1}] & [C_{J-1}]\\
 & & & [B_J] & [A_J]
\end{pmatrix}
\begin{pmatrix}
[\delta_1]\\ [\delta_2]\\ [\delta_3]\\ \vdots\\ [\delta_{J-1}]\\ [\delta_J]
\end{pmatrix}
= \begin{pmatrix}
[r_1]\\ [r_2]\\ [r_3]\\ \vdots\\ [r_{J-1}]\\ [r_J]
\end{pmatrix} \tag{38}$$

or

$$[A][\delta] = [r] \tag{39}$$

The elements of the matrices are given by

$$[A_j] = \begin{pmatrix}
1 & -h_j/2 & 0 & 0 & 0\\
(a_3)_{j-1} & (a_5)_{j-1} & (a_1)_{j-1} & (a_7)_{j-1} & 0\\
(b_3)_{j-1} & 0 & 0 & 0 & (b_1)_{j-1}\\
0 & -1 & -h_j/2 & 0 & 0\\
0 & 0 & 0 & -1 & -h_j/2
\end{pmatrix},$$

where $2 \le j \le J-1$ (40)

$$[C_j] = \begin{pmatrix}
0 & 0 & 0 & 0 & 0\\
0 & 0 & 0 & 0 & 0\\
0 & 0 & 0 & 0 & 0\\
0 & 1 & -h_j/2 & 0 & 0\\
0 & 0 & 0 & 1 & -h_j/2
\end{pmatrix}, \quad \text{where}$$

$1 \le j \le J-1$ (41)

$$[B_j] = \begin{pmatrix}
-1 & -h_j/2 & 0 & 0 & 0\\
(a_4)_{j-1} & (a_6)_{j-1} & (a_2)_{j-1} & (a_8)_{j-1} & 0\\
(b_4)_{j-1} & 0 & 0 & 0 & (b_2)_{j-1}\\
0 & 0 & 0 & 0 & 0\\
0 & 0 & 0 & 0 & 0
\end{pmatrix},$$

where $2 \le j \le J$ (42)

$$[\delta_j] = \begin{pmatrix}
\delta f_{j-1}\\ \delta u_{j-1}\\ \delta v_{j-1}\\ \delta g_{j-1}\\ \delta s_{j-1}
\end{pmatrix}, \quad \text{where} \quad 1 \le j \le J$$ (43)

https://doi.org/10.1021/acsomega.3c02949
ACS Omega 2023, 8, 29424−29436

$$[r_j] = \begin{pmatrix} (r_1)_{j-1/2} \\ (r_2)_{j-1/2} \\ (r_3)_{j-1/2} \\ (r_4)_{j-1/2} \\ (r_5)_{j-1/2} \end{pmatrix}, \quad \text{where} \quad 2 \le j \le J-1 \tag{44}$$

Finally, the LU method is utilized to decompose the system presented in eq 38 as

$$[A] = [L][U] \tag{45}$$

where

$$[L] = \begin{pmatrix} [I] & & & & \\ [\Gamma_2] & [I] & & & \\ & \ddots & \ddots & & \\ & & [\Gamma_{J-1}] & [I] & \\ & & & [\Gamma_J] & [I] \end{pmatrix} \tag{46}$$

and

$$[U] = \begin{pmatrix} [\alpha_1] & [C_1] & & & \\ & [\alpha_2] & [C_2] & & \\ & & \ddots & \ddots & \\ & & [\alpha_{J-1}] & [C_{J-1}] & \\ & & & [\alpha_j] & \end{pmatrix} \tag{47}$$

The matrices $[\alpha_i]$ and $[\Gamma_i]$ are both square matrices with dimensions of 5×5, while $[I]$ denotes the identity matrix. The step length is set to $\Delta y = h = 0.001$, and the calculation continues until the convergence criterion of $|\delta v_0^{(i)}| < \gamma$ is satisfied. Here, γ is a predetermined value chosen to indicate the level of acceptable convergence. Here, γ is chosen to be 0.00001 or 10^{-5}.

The following initial guesses have been chosen to initiate the computation

$$f_0(\eta) = \frac{-A_5 M_e}{3\eta_\infty^2}\eta^3 + \frac{(1 - \epsilon + A_5 M_e)}{2\eta_\infty}\eta^2 + \epsilon\eta - A_5 M_e \tag{48}$$

$$\theta_0(\eta) = g_0(\eta) = \frac{(1 - A_2 Pr\eta_\infty)}{\eta_\infty^2}\eta^2 + A_2 Pr\eta \tag{49}$$

5. RESULTS, VALIDATION, AND DISCUSSION

The study aimed to examine how various parameters impact a nanofluid that contains copper (Cu) nanoparticles dispersed in water, over a shrinking/stretching sheet with a melting surface. Specifically, we varied the melting parameter M_e over the range of 0−5, and the stretching/shrinking parameter ϵ from −1 to 2. We also examined the magnetic parameter M_g, radiation parameter Nr, copper nanoparticle concentration ϕ(ranging from 0 to 0.2), and mixed convection parameter (ranging from 0 to 0.5), while fixing the Prandtl number Pr at 6.8. The physical properties of the nanofluid, as well as the values of the constants used in the system, are provided in Tables 1 and 2. We extensively compared our results for $f''(0)$, Nusselt number, and skin friction coefficient with those obtained in previous studies,[18−21,40,43] across a range of values for the stretching/shrinking parameter ϵ, melting parameter M_e, and copper nanoparticle concentration ϕ (see Table 3).

Table 2. Thermophysical Properties of Water and Copper[39,40]

physical properties	symbols (units)	water (H_2O)	copper (Cu)
density	ρ (kg m^{-3})	997.1	8933
specific heat	C_p (J kg^{-1} K^{-1})	4179	385
thermal conductivity	k (W m^{-1} K^{-1})	0.613	400
thermal expansion	β (K^{-1})	21×10^{-5}	1.67×10^{-5}
electrical conductivity	σ (S m^{-1})	5.5×10^{-6}	58×10^{6}
dynamic viscosity	μ (Pa·s)	0.001	

Table 3. Effects of Different Parameters on the Values of $f''(0)$ and $g'(0)$

ϕ	ϵ.	M_e	Ri	M_g	Nr	$f''(0)$	$g'(0)$
0.0	0	0	0	0	0	1.23260	1.16614
0.01						1.26472	1.15822
	0.25					1.02612	1.41018
		1				0.96900	0.93225
			0.1			1.01339	0.94248
				1		1.24422	0.96755
					1	1.24735	0.85912
					2	1.25018	0.77518
				2		1.44881	0.78880
			0.2			1.46833	0.79293
		2				1.43107	0.69238
	0.75					0.53132	0.81287
0.05						0.54863	0.80759
0.1	−0.5	3	0.3	3	3	3.01947	0.47074

Our study focuses on various effects, and to compare our results with existing literature, we present the findings for melting, stretching, shrinking, local Nusselt number, and skin friction coefficient in Tables 4−66. These results, obtained by keeping other factors at zero, exhibit a remarkable degree of agreement with the existing literature. This substantiates the accuracy and reliability of our numerical approach, positioning it as the benchmark of our study. Consequently, researchers working in this field can confidently utilize our method with utmost assurance. As a reference for future studies, we have included a tabulation of the numerical solutions for $f''(0)$ and $g'(0)$, along with the values of the main parameters in Table 3.

This study presents the variation of $f''(0)$ and $\theta'(0)$ with respect to the shrinking/stretching parameter (ϵ) and melting parameter (M_e), as depicted in Figures 2 and 3, respectively. Moreover, the study also shows the changes in the local skin friction coefficient (Cf_x) and the local Nusselt number (Nu_x) in relation to the volume fraction (ϕ), M_e, and ϵ, as demonstrated in Figures 4−77. These figures reveal that an increase in the volume fraction ϕ leads to an increase in Cf_x, but a decrease in Nu_x. Conversely, an increase in the melting parameter M_e causes a decrease in Cf_x but an increase in Nu_x. Additionally, an increase in the shrinking/stretching parameter ϵ leads to a reduction in both the Nusselt number and the skin friction coefficient.

In Figure 8, the variation of velocity with different values of the stretching/shrinking parameter ϵ is depicted. It is evident from the figure that as the value of ϵ increases, the velocity also

https://doi.org/10.1021/acsomega.3c02949
ACS Omega 2023, 8, 29424−29436

Table 4. Analyzing of $f''(0)$ Values with Different Stretching ϵ and Melting M Parameters while Keeping Other Parameters at Zero

	Kishore Kumar and Bandari[21]				current result			
ϵ	$M_e = 0$	$M_e = 1$	$M_e = 2$	$M_e = 3$	$M_e = 0$	$M_e = 1$	$M_e = 2$	$M_e = 3$
0.0	1.232587	1.169659	1.137098	1.115590	1.232597	1.16957	1.13696	1.115421
0.1	1.146560	1.085575	1.054336	1.033811	1.146569	1.085493	1.054209	1.033655
0.2	1.051129	0.993238	0.963829	0.944592	1.051137	0.993162	0.963712	0.944449
0.5	0.713295	0.670793	0.649582	0.635841	0.71330	0.670741	0.649503	0.635745
1.0	0.000000	0.000000	0.000000	0.000000	0.000000	0.000000	0.000000	0.000000
2.0	−1.887301	−1.754887	−1.690853	−1.650111	−1.887316	−1.754753	−1.690651	−1.649868

Table 5. Validation of $f''(0)$ with Existing Literature for ϵ and Other Parameters Held at Zero

						present result		
$\epsilon = c/a$		ref 19	ref 40	ref 18	ref 20	$\phi = 0.0$	$\phi = 0.1$	$\phi = 0.2$
shrinking sheet	−0.25	1.402241		1.4022	1.40224	1.402253	1.647297	1.708013
	−0.5	1.495670	1.49567		1.49567	1.495685	1.757056	1.821819
	−0.75	1.489298		1.4893	1.48930	1.489316	1.749577	1.814064
	−1	1.328817	1.32881		1.32882	1.328840	1.561060	1.618600
	−1.05			1.2662		1.266253	1.487537	1.542367
	−1.15		1.08223	1.0822	1.08223	1.082262	1.271397	1.318261
	−1.2	0.932473	0.93247			0.932512	1.095483	1.135865
	−1.2465		0.58428		0.55430	0.584898	0.687377	0.712788

Table 6. Comparison of Local Nusselt Number and Skin Friction Values for Different ϕ and ϵ ($M_g = Nr = Ri = 0$, $Pr = 6.8$)

		Bachok et al.[43]		present result	
ϕ	ϵ	$\sqrt{Re_x}C_f$	$(Re_x)^{-1/2}Nu$	$\sqrt{Re_x}C_f$	$-(Re_x)^{-1/2}Nu$
0.1	−0.5	2.2865	0.8385	2.2865434	0.8400069
	0	1.8843	1.4043	1.8843441	1.4119916
	0.5	1.0904	1.8724	1.0904629	1.8850937
0.2	−0.5	3.1826	1.0802	3.1825860	1.0665224
	0	2.6226	1.6692	2.6227736	1.6245943
	0.5	1.5177	2.1577	1.5177891	2.0873790

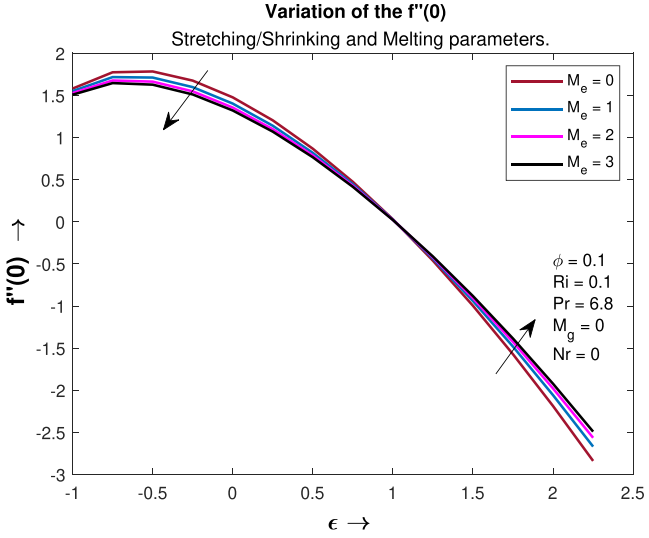

Figure 2. Effect of ϵ on $f''(0)$.

increases. It should be noted that ϵ is calculated as $\frac{c}{a}$. When ϵ is equal to 1, the free-stream velocity and the stretching velocity are the same, resulting in the formation of a uniform boundary layer. However, when ϵ exceeds 1, the free-stream velocity exceeds the stretching velocity, which causes the boundary layer to thicken. Conversely, when ϵ is less than 1, the stretching velocity exceeds the free-stream velocity, leading to an inverted boundary layer structure. These findings are consistent with the observations reported in Figure 2. Additionally, Figure 9 shows the temperature profile for different values of ϵ as a function of η, with increasing temperature as ϵ increases.

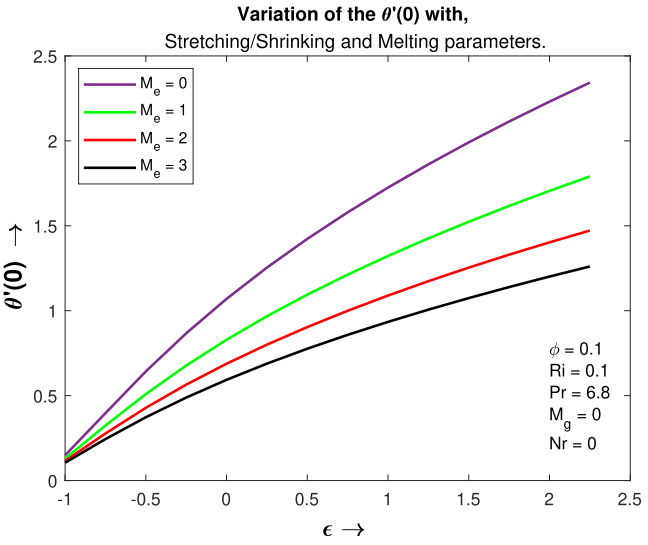

Figure 3. Effect of ϵ on $\theta'(0)$.

The velocity profile $f'(\eta)$ and temperature profile $\theta(\eta)$ are influenced by the melting parameter M_e, as depicted in Figures 10 and 11. The results indicate that as M_e increases, both profiles experience a decrease. This effect results from the fact that increasing the melting parameter improves the nanofluid's molecular motion while also causing a phase change. This phase transition causes a delay in momentum diffusion within the boundary layer, which inhibits all types of diffusion in the

https://doi.org/10.1021/acsomega.3c02949
ACS Omega 2023, 8, 29424−29436

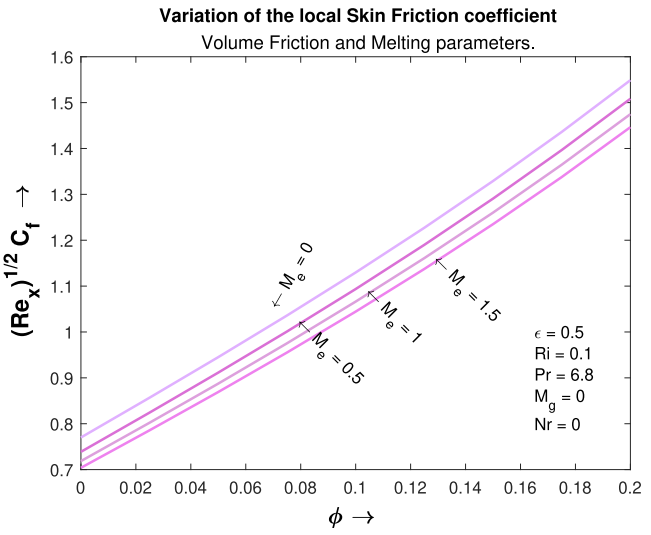

Figure 4. Effect of melting parameter M_e and ϕ on skin friction coefficient.

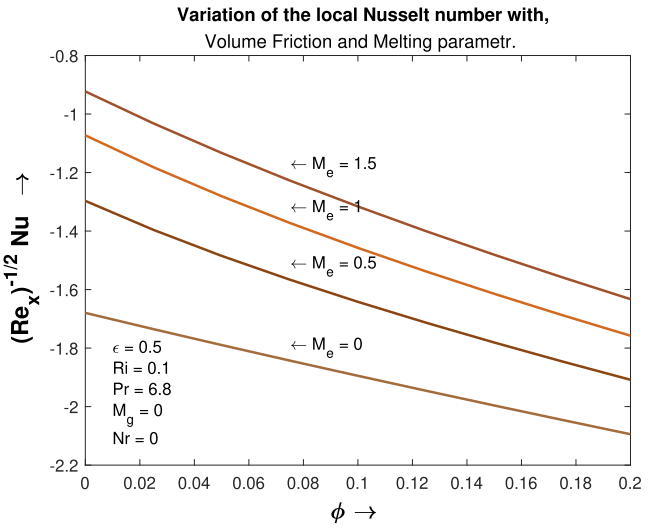

Figure 5. Effect of melting parameter M_e and ϕ on local Nusselt number.

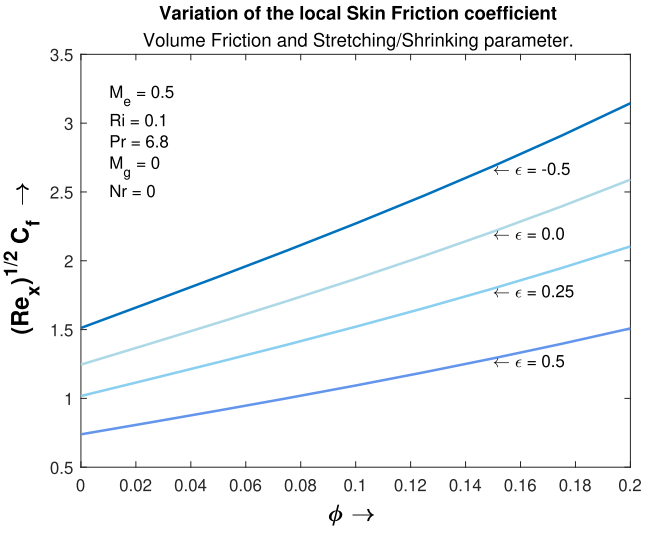

Figure 6. Effect of ϵ and ϕ on skin friction coefficient.

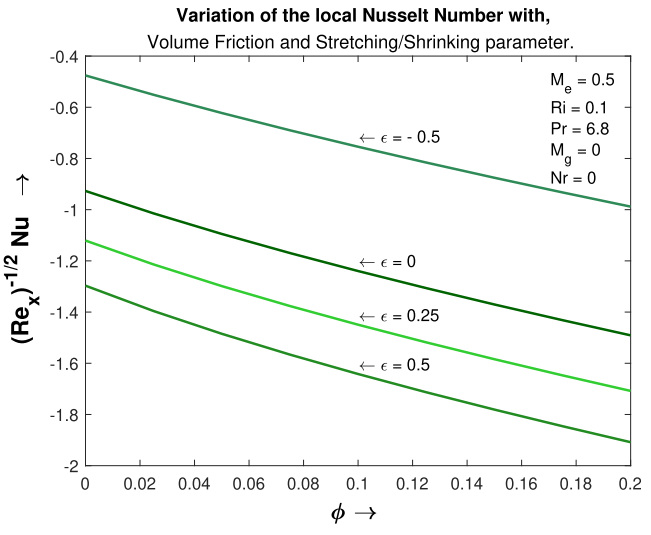

Figure 7. Effect of ϵ and ϕ on Nusselt number.

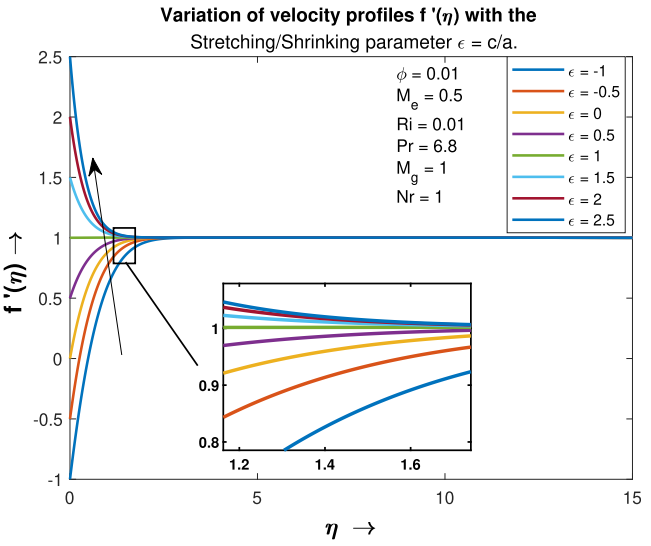

Figure 8. Effect of ϵ on f'.

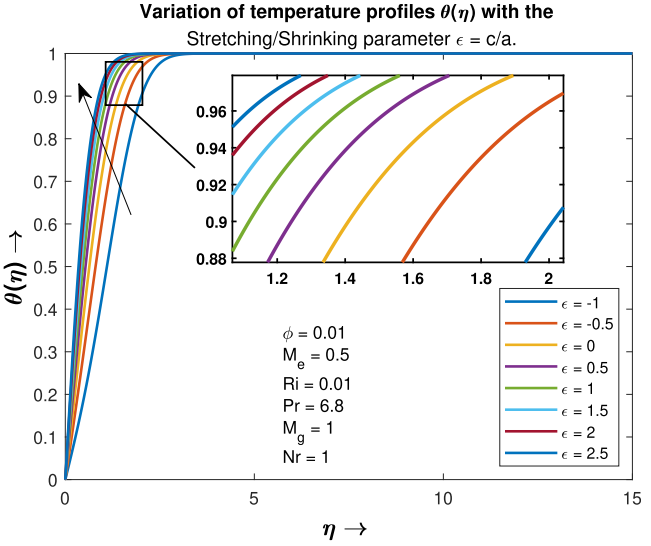

Figure 9. Effect of ϵ on θ.

https://doi.org/10.1021/acsomega.3c02949
ACS Omega 2023, 8, 29424−29436

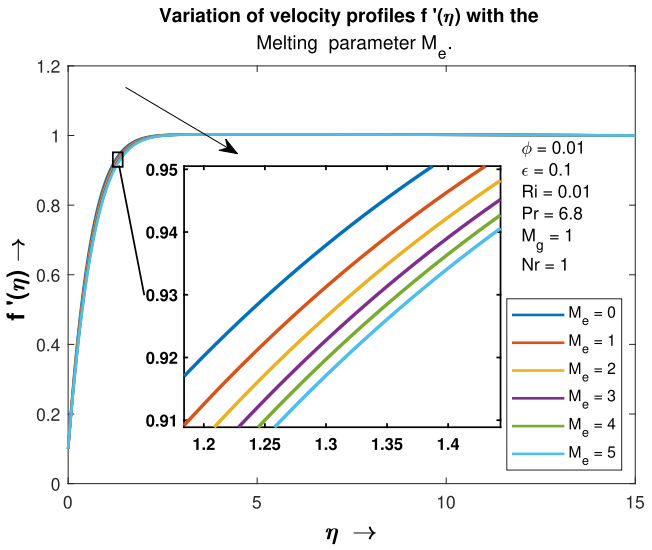

Figure 10. Effect of melting parameter M_e on velocity profile f'.

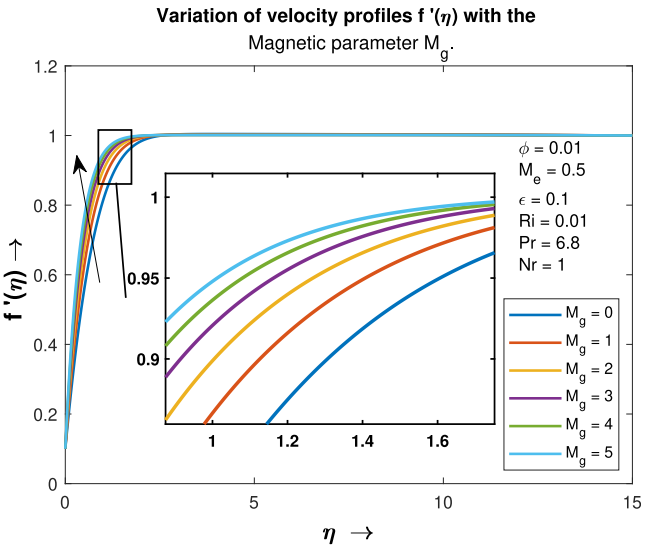

Figure 12. Effect of magnetic parameter M_g on f'.

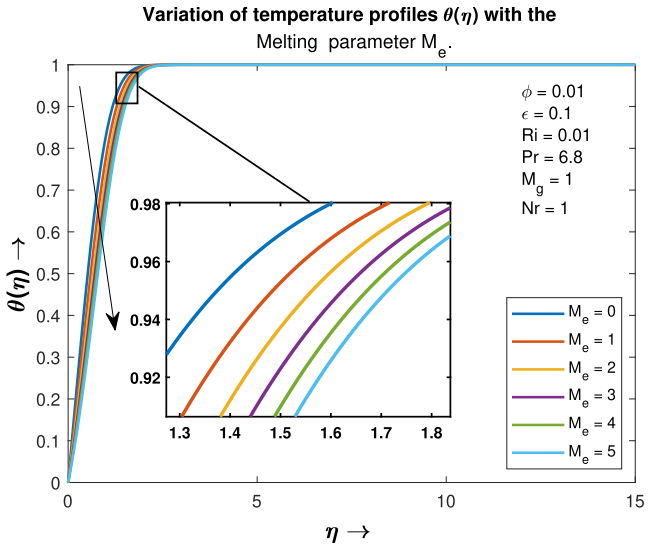

Figure 11. Effect of melting parameter M_e on θ.

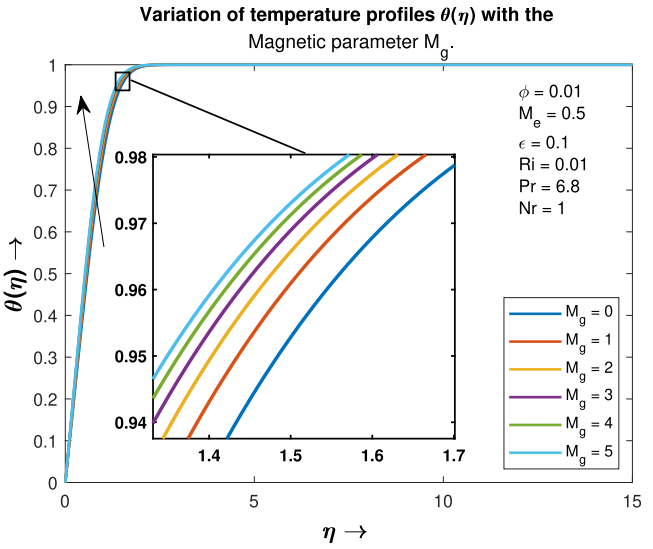

Figure 13. Effect of magnetic parameter M_g on θ.

thermal and momentum boundary layers, leading to reduced temperature and velocity profiles. Additionally, the thickness of the corresponding thermal boundary layer is reduced.

The velocity profile $f'(\eta)$ and temperature profile $\theta(\eta)$ are affected by the magnetic parameters M_g and mixed convection parameter Ri. These effects are depicted in Figures 12−1515, which show the directional relationship between the parameters and the profiles. Mixed convection is a phenomenon characterized by the Richardson number (Ri), which represents the balance between buoyancy forces and the external flow's inertia in heat and fluid transport. By increasing the mixed convection parameter, stronger buoyancy forces are generated, resulting in a more significant impact on the temperature and velocity fields. Consequently, the temperature and velocity fields are further enhanced. Figure 16 shows the impact of thermal radiation Nr on the temperature profile $\theta(\eta)$. The figure illustrates that increasing Nr causes a reduction in the temperature profile due to the enhanced transport of energy from the fluid to the surrounding environment by thermal radiation.

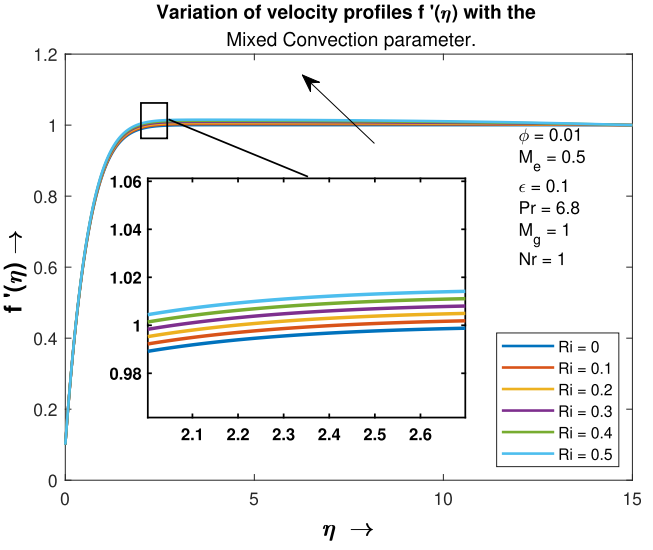

Figure 14. Effect of mixed convection parameter R_i on f'.

https://doi.org/10.1021/acsomega.3c02949
ACS Omega 2023, 8, 29424−29436

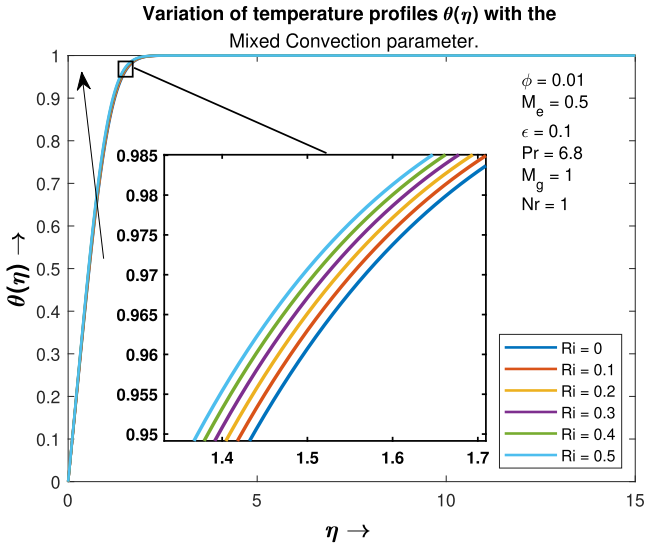

Figure 15. Effect of mixed convection parameter R_i on θ.

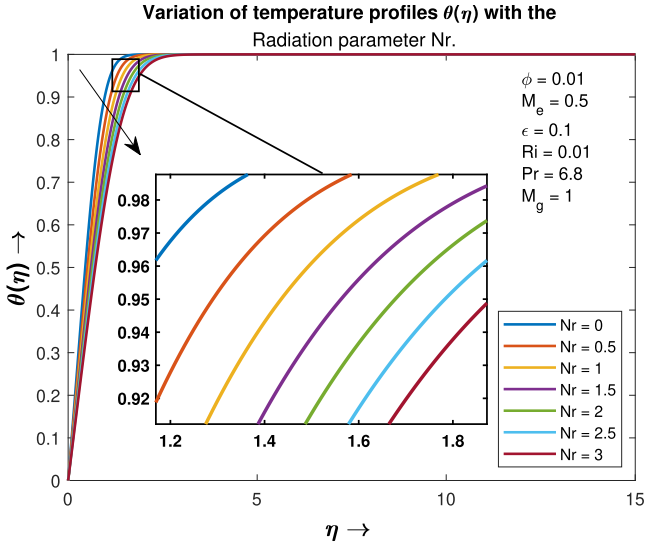

Figure 16. Effect of thermal radiation parameter N_r on θ.

6. CONCLUSIONS

This research delves into the impact of melting heat transfer on the steady, two-dimensional, laminar boundary layer of a nanofluid comprising Cu and water flowing over a stretching or shrinking sheet. The investigation scrutinizes the influence of key parameters, namely, the mixed convection parameter *Ri*, magnetic parameter M_g, and thermal radiation parameter *Nr*, on the skin friction coefficient (C_{fx}) and local Nusselt number (Nu_x), which reflect the shear stress and heat transfer, respectively. The numerical calculations are conducted using the Keller Box approach and MATLAB. The study provides valuable insights into the behavior of nanofluid exhibiting melting heat transfer in stagnation point flow and can be leveraged to optimize heat transfer systems across various engineering and industrial applications. The research presents a comprehensive analysis of diverse parametric scenarios, and the significant findings are succinctly summarized with respect to the controlling factors outlined in Table 3. Significant outcomes are listed as follows:

- The skin friction coefficient C_{fx} decreases as the melting parameter M_e and the shrinking/stretching parameter ϵ are increased, while the volume fraction ϕ increases the skin friction coefficient C_{fx}.
- The Nusselt number Nu_x rises as the melting parameter M_e does. However, as the volume fraction ϕ and the shrinking/stretching parameter ϵ grow, a decline in Nu_x is seen.
- The velocity profile decreases from the stagnation point at $\eta = 0$ to $\eta \to \infty$ when the stretching parameter ϵ is greater than 1, and increases from $\eta = 0$ to $\eta \to \infty$ when $\epsilon < 1$. The temperature profile θ increases as the stretching/shrinking parameter ϵ increases.
- The mixed convection parameter *Ri* leading to enhanced flow characteristics. As *Ri* increases, the profiles of temperature θ and velocity f' become more pronounced.
- The velocity profile f' and temperature profile θ both exhibit a decreasing trend as the melting parameter M_e increases.
- The temperature profile decreases as the thermal radiation parameter *Nr* increases, due to enhanced energy transport from the fluid to the environment.

AUTHOR INFORMATION

Corresponding Author

Yeou Jiann Lim − *Department of Mathematical Sciences, Faculty of Science, Universiti Teknologi Malaysia, 81310 Johor Bahru, Johor, Malaysia*; Email: jiann@utm.my

Authors

Arfan Hyder − *Department of Mathematical Sciences, Faculty of Science, Universiti Teknologi Malaysia, 81310 Johor Bahru, Johor, Malaysia; Department of Mathematics and Social Sciences, Sukkur IBA University, Sukkur 65200, Pakistan*; orcid.org/0000-0001-9780-5582

Ilyas Khan − *Department of Mathematics, College of Science Al-Zulfi, Majmaah University, Al-Majmaah 11952, Saudi Arabia*

Sharidan Shafie − *Department of Mathematical Sciences, Faculty of Science, Universiti Teknologi Malaysia, 81310 Johor Bahru, Johor, Malaysia*

Complete contact information is available at: https://pubs.acs.org/10.1021/acsomega.3c02949

Notes

The authors declare no competing financial interest.

ACKNOWLEDGMENTS

Special thanks go to the Higher Education Ministry of Malaysia and RMC (Research Management Centre) UTM for the funds' support via vote Q.J130000.3854.31J28 (UTM Encouragement Research). The authors appreciate all of the researchers and friends who have reviewed and suggested improving this article.

NOMENCLATURE

$(..)_f$	base fluid
$(..)_s$	solid nanoparticle
$(..)_{nf}$	nanofluid
α	thermal diffusivity (m^2/s)
β	thermal expansion
δ	boundary layer thickness

https://doi.org/10.1021/acsomega.3c02949
ACS Omega 2023, 8, 29424−29436

ϵ	stretching/shrinking parameter
η	similarity variable
γ	a dimensionless small quantity ($\ll 1$)
μ	absolute (dynamic) viscosity (N s/m^2)
ν	kinematic viscosity (m^2/s)
ϕ	the dimensionless solid volume fraction of hybrid nanofluid
ϕ	volume fraction
ψ	stream function
ρC_p	heat capacity (J/m^{3}K)
ρ	density (kg/m^3)
σ	electrical conductivity
τ	shear stress
θ	dimensionless temperature
A_1, A_2, A_3, A_4, A_5, A_6, a, c	constants
C_f	skin friction coefficient
C_p	specific heat (J/kg·K)
f	similarity variable
g	gravitational acceleration
k	thermal conductivity (W/m·K)
M_e	melting parameter
M_g	magnetic parameter
N_r	radiation parameter
Nu	Nusselt number
P	pressure (N/m^2)
Pr	Prandtl number
qr	radiation heat flux
Re	Reynolds number
Re_x	local Reynolds number
R_i	mixed convection parameter
T_∞	ambient temperature (K)
T_m	melting surface temperature (K)
T_s	temperature of the solid medium (K)
T_w	temperature of the surface plate (K)
u_e	free-stream velocity (ms^{-1})
u_w	velocity of the sheet (ms^{-1})

REFERENCES

(1) Choi, S. U.; Eastman, J. A. *Enhancing Thermal Conductivity of Fluids with Nanoparticles* Argonne National Laboratory: Argonne, IL; 1995.

(2) Alagumalai, A.; Qin, C.; Vimal, K.; Solomin, E.; Yang, L.; Zhang, P.; Otanicar, T.; Kasaeian, A.; Chamkha, A. J.; Rashidi, M. M.; et al. Conceptual analysis framework development to understand barriers of nanofluid commercialization. *Nano Energy* **2022**, *92*, No. 106736.

(3) Mahian, O.; Zhang, X.; Xu, B.; Yuan, M.; et al. Recent advances in modeling and simulation of nanofluid flows-Part I: Fundamentals and theory. *Phys. Rep.* **2019**, *790*, 1−48.

(4) Chakraborty, S.; Panigrahi, P. K. Stability of nanofluid: A review. *Appl. Therm. Eng.* **2020**, *174*, No. 115259.

(5) Li, J.; Zhang, X.; Xu, B.; Yuan, M. Nanofluid research and applications: A review. *Int. Commun. Heat Mass Transfer* **2021**, *127*, No. 105543.

(6) Krishna, M. V.; Ahammad, N. A.; Chamkha, A. J. Radiative MHD flow of Casson hybrid nanofluid over an infinite exponentially accelerated vertical porous surface. *Case Stud. Therm. Eng.* **2021**, *27*, No. 101229.

(7) Sreedevi, P.; Sudarsana Reddy, P.; Chamkha, A. Heat and mass transfer analysis of unsteady hybrid nanofluid flow over a stretching sheet with thermal radiation. *SN Appl. Sci.* **2020**, *2*, 1222.

(8) Roberts, L. On the melting of a semi-infinite body of ice placed in a hot stream of air. *J. Fluid Mech.* **1958**, *4*, 505−528.

(9) Yen, Y.-C.; Tien, C. Laminar heat transfer over a melting plate, the modified Leveque problem. *J. Geophys. Res.* **1963**, *68*, 3673−3678.

(10) Muhammad, T.; Waqas, H.; Farooq, U.; Alqarni, M. Numerical simulation for melting heat transport in nanofluids due to quadratic stretching plate with nonlinear thermal radiation. *Case Stud. Therm. Eng.* **2021**, *27*, No. 101300.

(11) Venkatadri, K.; Abdul Gaffar, S.; Rajarajeswari, P.; Prasad, V. R.; Anwar Bég, O.; Hidayathulla Khan, B. M. Melting heat transfer analysis of electrically conducting nanofluid flow over an exponentially shrinking/stretching porous sheet with radiative heat flux under a magnetic field. *Heat Transfer* **2020**, *49*, 4281−4303.

(12) Hayat, T.; Alsaedi, A.; et al. Development of bioconvection flow of nanomaterial with melting effects. *Chaos, Solitons Fractals* **2021**, *148*, No. 111015.

(13) Shettar, M. U.; Rudraiah, M.; Bragard, J.; Laroze, D. Induced Navieras Slip with CNTS on a Stretching/Shrinking Sheet under the Combined Effect of Inclined MHD and Radiation. *Energies* **2023**, *16*, 2365.

(14) Sakiadis, B. C. Boundary-layer behavior on continuous solid surfaces: I. Boundary-layer equations for two-dimensional and axisymmetric flow. *AIChE J.* **1961**, *7*, 26−28.

(15) Magyari, E.; Chamkha, A. J. Combined effect of heat generation or absorption and first-order chemical reaction on micropolar fluid flows over a uniformly stretched permeable surface: The full analytical solution. *Int. J. Therm. Sci.* **2010**, *49*, 1821−1828.

(16) Fang, T. Boundary layer flow over a shrinking sheet with power-law velocity. *Int. J. Heat Mass Transfer* **2008**, *51*, 5838−5843.

(17) Uddin, M.; Khan, W.; Ismail, A. M. Melting and second order slip effect on convective flow of nanofluid past a radiating stretching/shrinking sheet. *Propul. Power Res.* **2018**, *7*, 60−71.

(18) Mondal, H.; Bharti, S. Spectral quasi-linearization for MHD nanofluid stagnation boundary layer flow due to a stretching/shrinking surface. *J. Appl. Comput. Mech.* **2020**, *6*, 1058−1068.

(19) Jumana, S. A.; Murtaza, M.; Ferdows, M.; Makinde, O.; Zaimi, K. Dual solutions analysis of melting phenomenon with mixed convection in a nanofluid flow and heat transfer past a permeable stretching/shrinking sheet. *J. Nanofluids* **2020**, *9*, 313−320.

(20) Pop, I.; Roşca, N. C.; Roşca, A. V. MHD stagnation-point flow and heat transfer of a nanofluid over a stretching/shrinking sheet with melting, convective heat transfer and second-order slip. *Int. J. Numer. Methods Heat Fluid Flow* **2018**, *28*, 2089−2110.

(21) Kishore Kumar, Ch.; Bandari, S. Melting heat transfer in boundary layer stagnation-point flow of a nanofluid towards a stretching-shrinking sheet. *Can. J. Phys.* **2014**, *92*, 1703−1708.

(22) Gireesha, B.; Mahanthesh, B.; Shivakumara, I.; Eshwarappa, K. Melting heat transfer in boundary layer stagnation-point flow of nanofluid toward a stretching sheet with induced magnetic field. *Eng. Sci. Technol.* **2016**, *19*, 313−321.

(23) Kamal, M. H. A.; Ali, A.; Jiann, L. Y.; Rawi, N. A.; Shafie, S. Stagnation point flow of a hybrid nanofluid under the gravity modulation effect. *J. Adv. Res. Fluid Mech. Therm. Sci.* **2022**, *92*, 157−170.

(24) Alanazi, M. M.; Hendi, A. A.; Raza, Q.; Rehman, M. A.; Qureshi, M. Z. A.; Ali, B.; Shah, N. A. Numerical computation of hybrid morphologies of nanoparticles on the dynamic of nanofluid: The case of blood-based fluid. *Axioms* **2023**, *12*, 163.

(25) Rehman, S. U.; Fatima, N.; Ali, B.; Imran, M.; Ali, L.; Shah, N. A.; Chung, J. D. The Casson dusty nanofluid: Significance of Darcy-forchheimer law, magnetic field, and non-Fourier heat flux model subject to stretch surface. *Mathematics* **2022**, *10*, 2877.

(26) Hanif, H.; Shafie, S.; Rawi, N. A.; Kasim, A. R. M. Entropy analysis of magnetized ferrofluid over a vertical flat surface with variable heating. *Alexandria Eng. J.* **2023**, *65*, 897−908.

(27) Endalew, M. F.; Sarkar, S. Numerical exploration of forced convection hydromagnetic hyperbolic tangent nanofluid flow over a permeable wedge with melting heat transfer. *Sci. Rep.* **2023**, *13*, No. 3515.

https://doi.org/10.1021/acsomega.3c02949
ACS Omega 2023, 8, 29424−29436

(28) Mahat, R.; Saqib, M.; Khan, I.; Shafie, S.; Noor, N. A. M. Thermal radiation effect on Viscoelastic Walters'-B nanofluid flow through a circular cylinder in convective and constant heat flux. *Case Stud. Therm. Eng.* **2022**, *39*, No. 102394.
(29) Lim, Y. J.; Mohamad, A. Q.; Rawi, N. A.; Ling, D. C. C.; Zin, N. A. M.; Shafie, S. Analysis of Quadratic Thermal Radiation on Carreau Fluid Past a Melting Stretchable Cylinder, *Research Square* 2023, DOI: 10.21203/rs.3.rs-2432448/v1.
(30) Krishna, M. V.; Ahamad, N. A.; Chamkha, A. J. Hall and ion slip impacts on unsteady MHD convective rotating flow of heat generating/absorbing second grade fluid. *Alexandria Eng. J.* **2021**, *60*, 845−858.
(31) Krishna, M. V.; Chamkha, A. J. Hall and ion slip effects on MHD rotating flow of elastico-viscous fluid through porous medium. *Int. Commun. Heat Mass Transfer* **2020**, *113*, No. 104494.
(32) Krishna, M. V.; Chamkha, A. J. Hall and ion slip effects on MHD rotating boundary layer flow of nanofluid past an infinite vertical plate embedded in a porous medium. *Results Phys.* **2019**, *15*, No. 102652.
(33) Ali, B.; Nie, Y.; Hussain, S.; Habib, D.; Abdal, S. Insight into the dynamics of fluid conveying tiny particles over a rotating surface subject to Cattaneo-Christov heat transfer, Coriolis force, and Arrhenius activation energy. *Comput. Math. Appl.* **2021**, *93*, 130−143.
(34) Takhar, H. S.; Chamkha, A. J.; Nath, G. Unsteady laminar MHD flow and heat transfer in the stagnation region of an impulsively spinning and translating sphere in the presence of buoyancy forces. *Heat Mass Transfer* **2001**, *37*, 397−402.
(35) Singh, K.; Pandey, A. K.; Kumar, M. Numerical solution of micropolar fluid flow via stretchable surface with chemical reaction and melting heat transfer using Keller-Box method. *Propul. Power Res.* **2021**, *10*, 194−207.
(36) Ilias, M. R. Steady and Unsteady Aligned Magnetohydrodynamics Free Convection Flows of Magnetic and Non Magnetic Nanofluids along a Wedge, Vertical and Inclined Plates. Thesis; Universiti Teknologi Malaysia, 2018.
(37) Dawar, A.; Shah, Z.; Khan, W.; Idrees, M.; Islam, S. Unsteady squeezing flow of magnetohydrodynamic carbon nanotube nanofluid in rotating channels with entropy generation and viscous dissipation. *Adv. Mech. Eng.* **2019**, *11*, No. 1687814018823100.
(38) Hanif, H.; Shafie, S. Interaction of multi-walled carbon nanotubes in mineral oil based Maxwell nanofluid. *Sci. Rep.* **2022**, *12*, No. 4712.
(39) Makinde, O. D.; Mutuku, W. N. Hydromagnetic thermal boundary layer of nanofluids over a convectively heated flat plate with viscous dissipation and ohmic heating. *UPB Sci. Bull., Ser. A* **2014**, *76*, 181−192.
(40) Pal, D.; Mandal, G. Mixed convection-radiation on stagnation-point flow of nanofluids over a stretching/shrinking sheet in a porous medium with heat generation and viscous dissipation. *J. Pet. Sci. Eng.* **2015**, *126*, 16−25.
(41) Kakar, N.; Khalid, A.; Al-Johani, A. S.; Alshammari, N.; Khan, I. Melting heat transfer of a magnetized water-based hybrid nanofluid flow past over a stretching/shrinking wedge. *Case Stud. Therm. Eng.* **2022**, *30*, No. 101674.
(42) Cebeci, T.; Bradshaw, P. *Physical and Computational Aspects of Convective Heat Transfer*; Springer Science & Business Media, 2012.
(43) Bachok, N.; Ishak, A.; Pop, I. Stagnation-point flow over a stretching/shrinking sheet in a nanofluid. *Nanoscale Res. Lett.* **2011**, *6*, 623.

https://doi.org/10.1021/acsomega.3c02949
ACS Omega 2023, 8, 29424−29436